COMBINING PHOTOGRAMMETRY AND LASER SCANNING FOR DEM GENERATION IN STEEP HIGH-MOUNTAIN AREAS

M. Züblin[a,] *, L. Fischer[b] and H. Eisenbeiss[a]

[a]Institute of Geodesy and Photogrammetry, ETH Zurich, 8093 Zurich, Switzerland, +41 44 633 32 87 - zueblinm@ethz.ch, ehenri@geod.baug.ethz.ch
[b]Glaciology, Geomorphodynamics and Geochronology, Department of Geography, University of Zurich, 8057 Zurich, Switzerland, + 41 44 635 51 19 - luzia.fischer@geo.uzh.ch

Youth Forum

KEY WORDS: DEM/DTM, LiDAR, Image Matching, Glaciology, Landslides, Snow Ice, Change Detection, Orientation, Multitemporal

ABSTRACT:

This study presents the processing of both aerial and oblique images as well as LiDAR data of the Monte Rosa east face, an extremely challenging environment in the European Alps due to the height, steepness and ice coverage of the rock wall. New techniques of airborne LiDAR data acquisition are combined with established photogrammetric processing methods of aerial images to develop high-resolution DEMs for different epochs since 1956. Furthermore, a novel approach for DEM generation from helicopter-based oblique photos is introduced. Different software solutions for image processing and DEM generation are used and evaluated for applications in such steep high-mountain terrain. Reliability and accuracy as well as usability of the different data sets is shown and finally DEM subtractions give an insight in the strong topographic changes in the Monte Rosa east face within the investigated timeframes.

1. INTRODUCTION

The Monte Rosa east face, Italian Alps, is one of the highest flanks in the Alps (2200–4600m a.s.l.). Steep hanging glaciers and permafrost cover large parts of the wall. Since the end of the Little Ice Age (about 1850 AD), the hanging glaciers and firn fields have retreated continuously. During recent decades, the ice cover of the Monte Rosa east face experienced an accelerated and drastic loss in extent. Some glaciers have completely disappeared. New slope instabilities, detachment zones of gravitational mass movements developed, enhanced rock fall and ice avalanche activity were observed (Kääb et al., 2004; Fischer et al., 2006).

Figure 1: Monte Rosa east face, seen from Monte Moro

Mass movement processes have taken place all times because of the height and steepness of the Monte Rosa east face. Over the recent two decades, however, the mass movement activity in the Monte Rosa east face has drastically increased and several large rock and ice avalanche events occurred. In August 2005, an ice avalanche with a volume of more than $1x10^6$ m^3 occurred and in April 2007, a rock avalanche of about $0.3x10^6$ m^3 detached from the upper part of the flank (Fischer et al., 2006).

For the investigation of the Monte Rosa east face, remote sensing based techniques are crucial due to the inaccessibility of wide areas of the rock wall. Steep and high rock walls are an extremely challenging environment for effective data collection. This study is done within a pilot project for multidisciplinary investigations of such large and steep high-mountain flanks integrating different investigation techniques and data sets to achieve exacting spatial and temporal resolution. DEMs represent the core of most investigations of high-alpine flanks and they are crucial for geomorphic and morphometric analyses. A highly promising, yet in high-mountain areas rarely exploited method is the coupling of laser scanning data with photogrammetric analyses of terrestrial and aerial images, to extract topographic features and changes from DEMs.

Main objective of this paper is the investigation of DEMs developed with different methods for different times, with regard to accuracy and their usability for investigations of the drastic changes in glaciers and bedrock in the Monte Rosa east face.

2. DATA SETS

Available data sets for the Monte Rosa east face are terrestrial images, aerial images and high-resolution laser scanning data

(Tab. 1). Aerial images in image scales of about 1:12'000 to 20'000 (acquired by swisstopo) are available back to 1956 and the latest image was taken in 2007, but since we had other data available in the years 2005 and 2007, the most recent aerial image we used was from 2001. Such swisstopo aerial images in similar quality and time intervals are available for the whole area of Switzerland, making it a ready archive for assessments of other areas of interest.

The acquisition geometry in steep terrain is very unfavourable for traditional aerial images, therefore the usage of other data was considered. Terrestrial images were also available with different acquisition times but they were taken by various people with several uncalibrated cameras. A photogrammetric evaluation under these circumstances would be quite difficult and laborious, thus these images were used for interpretations in combination with generated DEMs without processing.

Figures 2 and 3 show a comparison of the same detailed outcrop in the different optical data sets. The quality of the images varies significantly between the aerial images from 1956 to 2001. Furthermore, the images taken with the helicopter allow the detection of more features, since these images have a larger image scale than the analog aerial images.
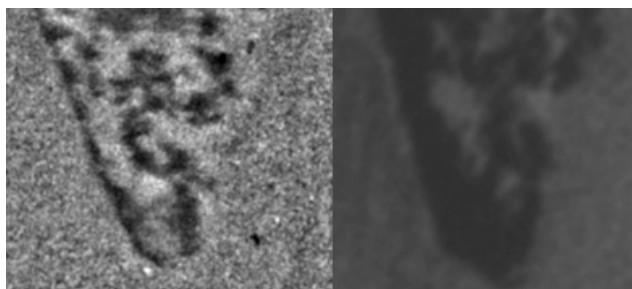

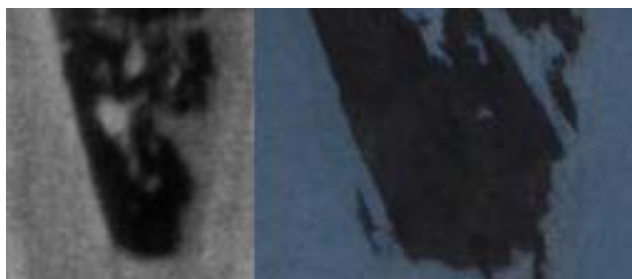Figure 2: Comparison of aerial imagery from 1956 (left) and 1988 (right).

Figure 3: Comparison of aerial imagery from 2001 (left) and colour image taken from the helicopter from 2007 (right).

Both laserscanning and optical data (oblique images) for 2007 were acquired by a manned helicopter. The used Helimap system by UW+R SA (Vallet, 2007; Vallet & Skaloud, 2004) is a handheld acquisition unit that can be installed on standard helicopters. The acquisition system determines the position and attitude of itself using a GPS/INS combination.

For normal use, the system relies on a Riegl LMS-Q240i-60 Laserscanner for point cloud generation. It can acquire up to 10'000 points per second with a maximal range of 300 to 400 meters. The Riegl scanner is ruggedized for airborne use and

allows the LiDAR measurements to be synchronized with the GPS/INS unit. The range measurement principle is pulsed time-of-flight. The images – normally used for texture mapping but in this project for DEM generation too – are acquired using a Hasselblad H1 camera with a Dos Imacon Xpress 22Mpix back. The CCD-sensor has a size of 49x37mm resulting in a pixel size of 9 μm. Both sensors have a similar field of view (57° for the camera and 60° for the LiDAR).

The IMU is a tactical-grade strapdown inertial system (iMAR LMS) with a very high measurement rate (up to 500 Hz). The GNSS-signal is received by a carrier phase receiver. Main advantage of the system compared to conventional aerial systems lies in its image acquisition geometry. Due to the fact that the system can be tilted, the acquisition configuration can be adapted even for steep terrain. Oblique images have the same beneficial properties as nadir zenith images. Additional electronics are used to synchronize all sensors.

LiDAR data acquired by the Swissphoto Group with an ALTM3100 System from Optech are available for 2005. The LiDAR sensor is mounted on a fixed wing aircraft. A Trimble GPS receiver and Applanix POS-AV are used to obtain position and orientation. The system was already used for data acquisition for an area of more than 50'000 km^2, but usually not in altitudes over 2000m as in this project.

Date of Acquisition	Type of Data	Amount of Data	Area [km^2]
Sept. 2007	Helicopter-based LiDAR	$4.8*10^6$ points	3
Sept. 2007	Helicopter-based oblique images	~300 22 MPixel images (not all used)	3
July & October 2005	Airplane-based LiDAR	$18.5*10^6$ points	5
Sept. 2001	Aerial images	3 images, scale ~1:20'000	~20
Sept. 1988	Aerial images	4 images, scale ~1:20'000	~25
Sept. 1956	Aerial images	3 images, scale ~1:12'000	4

Table 1: Facts about the available data sets.

3. PROCESSING OF IMAGE DATA

3.1 Software Packages

For the orientation of the images three different Software packages were evaluated: LPS (Leica Photogrammetry Suite 9.1 Build 282), the embedded ORIMA (Orientation Management Software, ORIMA-LPS-M Rel. 9.10) and ISDM (Z/I Imaging, Image Station Digital Mensuration Version 04.04.17.00). For the DEM generation the in-house developed software package SAT-PP (Satellite imagery Precise Processing) was used.

LPS was used successfully for the orientation of the aerial images from swisstopo, the Helimap Images could only be oriented properly with ISDM.

The three different software systems follow different approaches for the tie point measurements in the image. ORIMA is left out as we relied on LPS – where ORIMA is embedded – for point measurement.

LPS allows processing imagery from a wide variety of sources and formats (e.g. satellite, aerial and close range images). It contains modules for data import, input and export, image viewing, camera definitions, GCP and tie point measurements, triangulation, orthorectification and DEM generation. The camera calibration and the known interior orientation of these cameras can be inserted. For the calculation of the exterior orientation parameters, a triangulation of the image block has to be done. Therefore, ground control points (GCPs) have to be measured manually. The tie point measurement method depends on the input data and the terrain, under good conditions the automatic measurement tool can be used.

The LPS standard point measurement uses a screen with two triple tiled windows showing different zoom levels for each image. In ISDM such windows (usually two per image plus possibly one in stereo) can be freely arranged. A negative point would be that each window has a title bar of its own that takes up valuable display space.

A big difference – felt mainly in manual blunder detection – is that ISDM can simultaneously display more than two images (seems to be restricted by available memory, too large number of simultaneously opened images can cause crashes) while LPS only allows multi-image display in stereo mode. When a point is displayed in five different images simultaneously it can be corrected in all the images at the same time. Moreover, if an erroneous measurement occurred only in one image there is no possibility to determine which one is the false with only two images.

ISDM includes a matching algorithm directly implemented in the point measurement. When it is activated by clicking in an image ISDM tries to match the currently active point in this image taking the cursor position as initial value. The results are usually usable but a gain in productivity depends a lot on the individual user, especially inexperienced users could profit a lot from this feature. The possibility to calculate a relative orientation in ISDM is also advantageous for blunder detection or reaffirmation that there are currently no blunders. In LPS a blunder can be detected only by manual checking until the project has proceeded to the point where a bundle adjustment is possible. After finishing just one model in ISDM a relative orientation can confirm whether the measured points are correct and accurate.

3.2 Traditional Aerial Imagery

The orientation of the aerial images was performed in LPS to recover the exterior parameters of the camera. Ground control points (GCP) and a number of tie points were measured manually. Because of the large distortion of the images due to the steepness of the rock wall, no automatic extraction of tie points was possible. For 2001 and 1988 image blocks of three aerial images were used, for 1956 a block of four aerial images.

DEM	σ_0 [Pixel]	Control Point RMSE [m, resp. Pixel]
2001	0.48	X: 1.3, Y: 0.6, Z: 1.5 x: 0.21, y: 0.57
1988	0.60	X: 1.9, Y: 1.3, Z: 2.5 x: 0.15, y: 0.66
1956	0.99	X: 1.6, Y: 1.5, Z: 1.7 x: 0.62, y: 0.34

Table 2: Orientation of the aerial images with LPS.

Because of the lack of survey points in the Monte Rosa east face, the coordinates of the GCPs were extracted from topographic maps (1:25'000) and height notations in the map, both produced by swisstopo. Therefore, existing buildings as alpine huts and prominent and unmovable features like rock corners were measured. This induces an absolute accuracy of control points in planimetry and height of 1 to 2 m. However, the accuracy of the image point measurement results in half of a Pixel, which shows the high quality of the orientation considering the height and steepness of the rock wall (Table 2). The variances of the σ_0 value from 0.48 to 0.99 Pixel respectively from 2001 to 1956 is explainable with the image quality. The image quality, as mentioned above, is better for the more recent aerial images, therefore the point measurements are more accurate. Finally, the exterior camera orientation parameters were exported from LPS for subsequent image matching and DEM generation in SAT-PP.

3.3 Oblique Photos

The orientation of the oblique images was not conducted at high absolute precision, since the resulting point cloud will be transformed with LS3D relative to the LiDAR data. Tie points were manually and automatically measured as well as visually checked in LPS.

From the GPS/INS measurements initial exterior orientation parameters are available. They even allowed stereo viewing of the images with a y-parallax, which results from the accuracy level of the GPS/INS-system. Therefore, by using only the given exterior orientation the processing of the images were not possible.

GCPs were generated by identifying common points in the LiDAR data and the oblique images. With this method no high accuracy can be achieved. But as further analysis will be done by registration of the resulting point cloud with other point clouds in LS3D anyway no high absolute accuracy was needed. With LPS it was not possible to calculate an exterior orientation, neither with GCPs (up to 14) alone nor with supplementary exterior orientation information. The bundle block adjustment did not only terminate but also yielded very erroneous results (e.g. negative RMSE values). In our opinion the optimisation of the bundle adjustment or some basic implementation of it can not cope with the oblique geometry that also is not constant over the whole block. The orientation angles change a lot between single images as the helicopter trajectory is not as stable as the one of a fixed-wing airplane and the helicopter position was adapted to the mountain (e.g. change of orientation to see otherwise occluded parts of the rock-face).

Unfortunately, in LPS no relative orientation can be calculated separately, therefore a relative orientation with ORIMA was attempted. Here, only single models could be calculated, the

relative orientation of the whole block failed. Also tests with exterior orientation parameters, GCPs, free-network adjustment or minimal datum were unfruitful.

Therefore, a software was written to transfer the tie points from the LPS image coordinates (in Pixel) to ISDM image coordinates (in μm). In this step, also different orientations and centers of the image coordinate system had to be taken into account. SAT-PP uses the top-left corner of a pixel as origin and coordinate axes facing down and right whilst all these properties can be chosen freely in ISDM.

In ISDM, a relative as well as an absolute orientation could be computed. Because of the planned registration in LS3D we settled for an exterior orientation with an almost minimal datum (3 GCPs with a defined large a priori standard deviation (5m)) to avoid wrong constraints trough the artificial GCPs.
The results in Table 3 show that the relative orientation is not diminished by the addition of 3 GCPs but also that the accuracy of the GCPs is low. The standard deviation of the relative orientation is with 3.8 μm clearly smaller than one pixel (9 μm).

Orientation	σ_0 in image space [μm]	RMS of control points [m]
Relative	3.80	-
Absolute with 3 GCPs	3.81	X: 2.9 Y: 1.0 Z: 3.4

Table 3: Accuracy of orientations obtained with ISDM.

3.4 DEM Generation

The image matching and DEM generation from the aerial images was done in SAT-PP (Satellite image Precision Processing, ETH Zurich). Main component of this software package is the multiple image matching algorithm for the extraction of image correspondences and the generation of 3D data. The approach uses a coarse-to-fine hierarchical solution with an effective combination of several image matching algorithms and automatic quality control (Zhang, 2005, Wolff & Gruen, 2007). The extraction and matching of feature points, grid points as well as edges produces high amount of information for the subsequent DEM generation, which can be done with pixel level accuracy. Detailed mathematical descriptions of the SAT-PP software package are given in Zhang & Gruen (2006), Gruen et al. (2005), Zhang (2005).

In preparation of the automatic point extraction and matching process of the aerial images, a minimum of 4 seed points had to be measured manually in each stereo-pair of the image blocks. Due to the complex and steep topography as well as the widespread ice coverage, a ten times higher number of points had to be measured than in flat and ice-free aerial images. With this additional manual measuring support, the automatic point extraction worked efficient.

Grid spacing of the generated DEMs is 2m (2-4 pixels) for the aerial images. Main problems and blunders in the DEM occur in shadow areas, oversteepened zones and also on totally white glacier surfaces. The problem in these zones is the lack of enough contrast to detect feature points and edges for the matching. Improvements could be reached by enhanced manual measurements of seed points as well as lines along the plumb line.

4. PROCESSING OF LIDAR DATA

After a filtering of the raw data, the LiDAR point clouds were processed in SCOP++. The filtering of the LiDAR point clouds was quite simple as there is no vegetation and no buildings. Artefacts such as points in air (birds or parts of the helicopter) and points far beneath ground surface were eliminated.

The SCOP++ software derives a DEM from a point cloud and it is designed for the processing of very high amounts of points. SCOP++ performs filtering of airborne laser scanning data for automatic classification of the raw point cloud into terrain and off-terrain points, i.e. for extracting the true ground points for further DTM processing. It uses efficient robust interpolation techniques with flexible adaptation to terrain type and terrain coverage. The 2005 and 2007 LiDAR data was processed with the automatic LiDAR classification tool. Resolution of the output grid is 2m, as the photogrammetric derived DEMs are also calculated with a 2m resolution. For both LiDAR data sets, also DEMs with 1m resolution were calculated. In this resolution, stripes from the scanning process were visible, further processing has to be done for the application of 1m or even better resolution. This has not been done yet as the resolution of 2m is sufficient for this study.

5. REGISTRATION AND COMPARISON

Due to the lack of accurate GCPs in the rock wall for the image orientation, the photogrammetrically derived DEMs show offsets of several meters (Table 4). Therefore, the produced DEMs must be transformed into a common coordinate system. The LiDAR DEM acquired in 2007 serves as reference. Automatic co-registration of DEMs was conducted with LS3D (Least Squares 3D Matching; Akca and Gruen, 2007). The LS3D method estimates the transformation parameters of one DEM to a reference one, using the Generalized Gauss-Markoff model, minimizing the sum of squares of the Euclidean distances between the surfaces (Gruen and Akca, 2005). This method is a one step solution for the matching and georeferencing of multiple 3D surfaces that are globally matched and simultaneously georeferenced. By this step, the accuracy of the different photogrammetrically derived DEMs can be assessed as well as the accuracy of the two LiDAR DEMs.

The σ_0 of the comparisons between the 1988 respective 1956 and the 2007 LiDAR DEM is clearly larger than the σ_0 of the respective registration. This is due to the fact that for the registration, large blunders and also large topographic changes are not used and for the comparison, these large differences are included. The σ_0 of registration and comparison of the 2001 and 2005 DEM are more consistent, that confirms the better quality of these DEMs as well as less topographic changes within these two short periods.

DEM	σ_0 of registration [m]	σ_0 of comparison [m]
2005	1.7	2.4
2001	3.9	4.3
1988	4.5	16.3
1956	5.4	19.4

Table 4: Registration and comparison of the photogrammetric DEMs with the 2007 LiDAR DEM.

6. RESULTS

The subtraction of the different DEMs revealed impressively the topographic changes in ice and bedrock that occurred within the investigated epochs. Terrain changes could be quantified and dated accurately and quantitative volumetric estimations of mass loss and/or mass accumulation could be computed. Furthermore, the detachment zones of rock and ice avalanche events could be localized.

In the time period between 1988 and 2007 (see Figure 4) large mass loss with vertical terrain changes up to 120m can be observed. The main part of the mass loss occurred in ice but also some in bedrock. Visible accumulation corresponds to changes in glaciers length. Smaller accumulations might have been overlaid by the general trend of mass loss in this area.

In the short biannual time period of 2005 to 2007 (see Figure 5) the results are quite different. Both mass loss and accumulation occur. Most of the positive vertical terrain change correspond to glacier movements and ice accumulation. These changes of mass are within the expected normal changes of a hanging glacier. In the upper-left part of the image a detachment zone of a rock fall event was detected with a vertical surface change of over 30 meters.
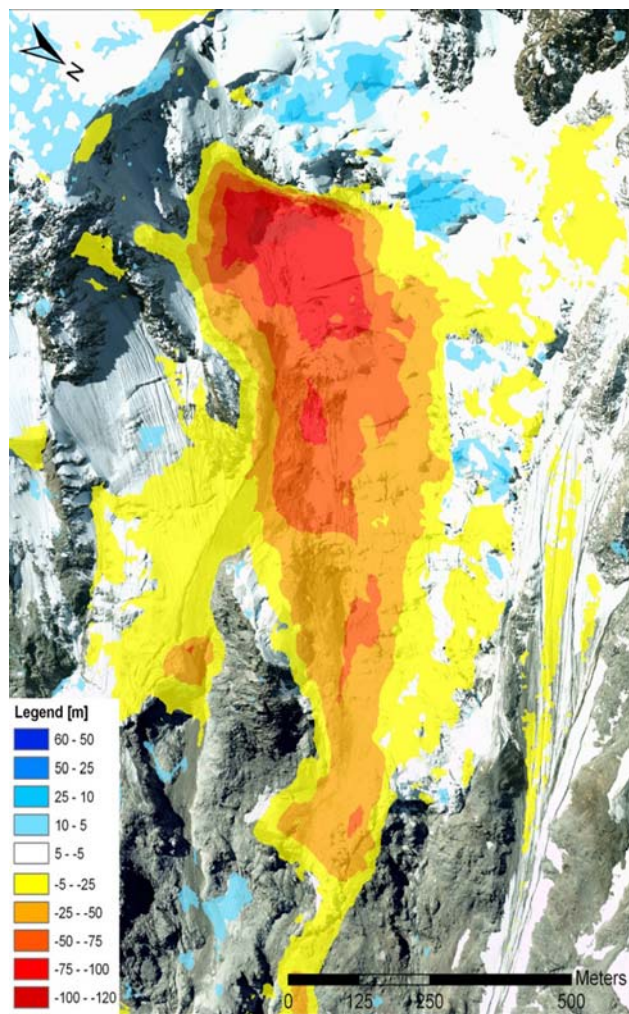

Figure 4: DEM comparison between the photogrammetric DEM from 1988 and the 2007 LiDAR DEM.
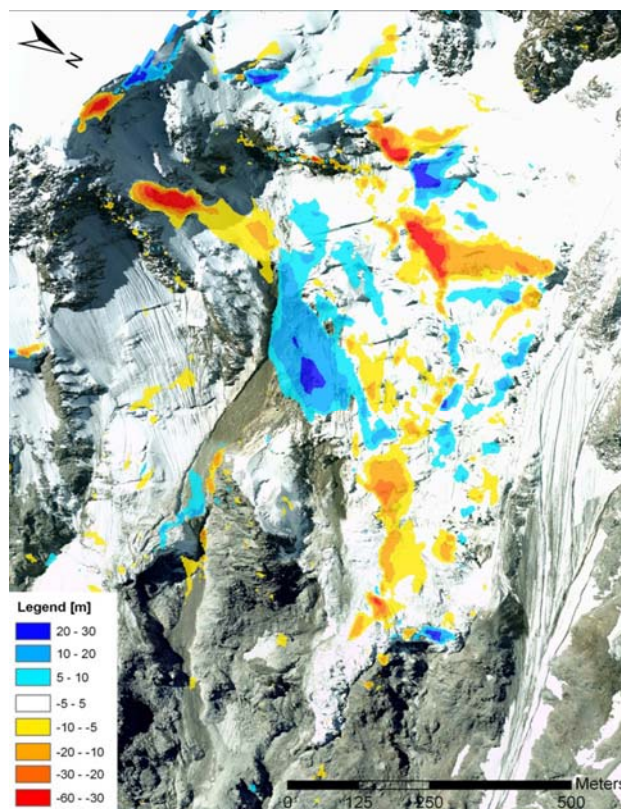

Figure 5: DTM comparison between the two LiDAR DEMs from 2005 and 2007.

7. CONCLUSION & PERSPECTIVES

The comparison of the different types of DEMs shows, that the processing of aerial images with SAT-PP results in DEMs that have comparable quality and high point density as LiDAR data. The major quality reduction of the 1956 image orientation and DEM results from the image quality. However, the combination of LiDAR data and photogrammetric methods is a valuable tool to enhance data set and temporal resolution. Moreover, DEMs with considerably more points can be generated by the photogrammetric processing of the oblique photos.

These higher-resolution DEMs could be used for more detailed analysis. Also the photogrammetric modelling allows the detailed and exact determination of edges which is impossible from LiDAR data. These edges are relevant to recognize and extract topographical and geological structures from steep rock walls such as the Monte Rosa east face.

The comparison of the different DEMs allowed some outlook on their reliability and accuracy. Naturally no check points for the older aerial images could be measured to assess their quality. But the matching with LS3D and subsequent analysis of the differences as well as comparisons with terrestrial images showed that the generated DEMs are reliable. As for the generation of the DEMs from the oblique images no GPS/INS information was used, this DEMs can be considered as independent data additionally to the helimap LiDAR data. The comparison with LS3D shows that both are without gross errors. The differences between the LiDAR DEM and the DEM derived from the oblique images result from the occlusions of particular parts of the cliff (see Figure 6), which could not be

detected with the laser scanning. Furthermore, looking at the raw point cloud a great variance of the distances between the single laser lines is visible (see Figure 7). These artefacts did not occur in the DEM derived from images (see Figure 8), since the high image overlap allowed the DEM generation in the above mentioned problematic area.
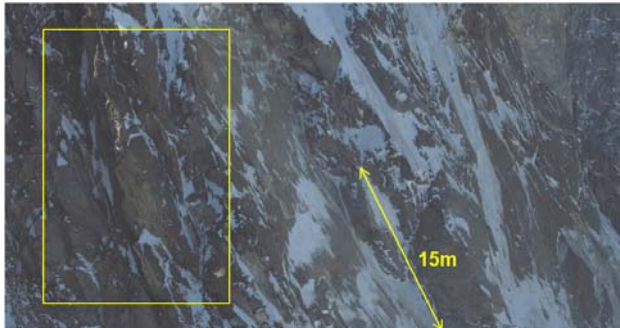

Figure 6: Zoom-in for one of the oblique images in a shadow area of the cliff. The highlighted rectangle shows an area, which partly could not be acquired with the LiDAR-system.

The results of the surface modelling from the oblique images shows, that because of the large image scale and the high overlap of the images, the DEM shows less holes and more details of the surface.

In future work we will analyse the accuracy of the DEMs more in detail. Furthermore, we will evaluate all DEMs with respect to the detection of terrain movements. The focus of our investigations will be on the analysis of small structures, which are visible in the DEM generated out of the oblique images.
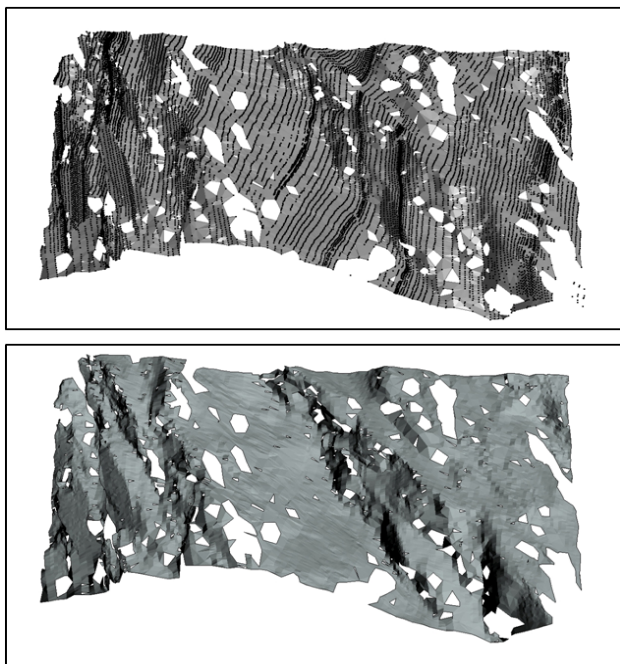

Figure 7: The upper part shows the LiDAR point cloud, while the lower part shows a surface model of the point cloud with 50cm resolution.
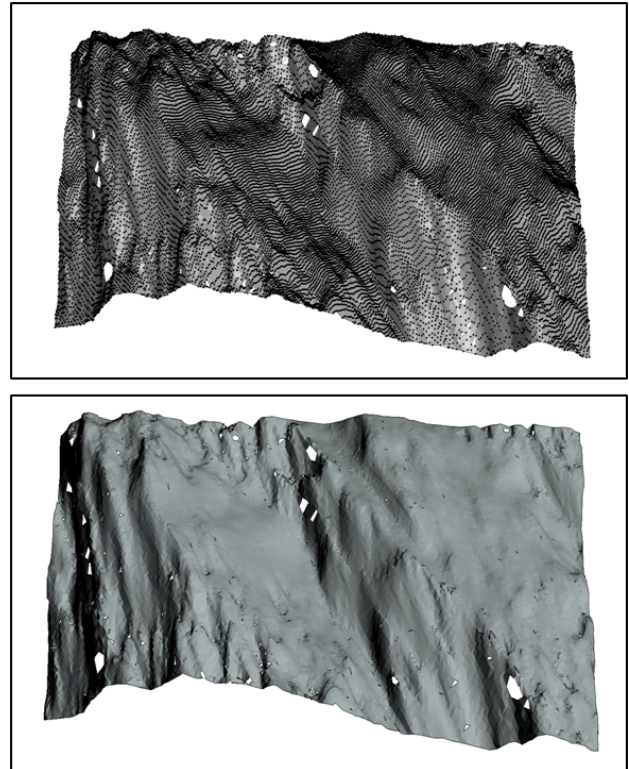

Figure 8: The upper part shows the matching point cloud (oblique images), while the lower part shows a surface model of the point cloud with 50cm resolution.

REFERENCES

Akca, D. & Gruen, A., 2007. Generalized least squares multiple 3D surface matching. *IAPRS Volume XXXVI,* Part 3/W52.

Fischer, L., Kääb, A., Huggel, C. & Noetzli, J., 2006. Geology, glacier retreat and permafrost degradation as controlling factors of slope instabilities in a high-mountain rock wall: the Monte Rosa east face. *Natural Hazards and Earth System Sciences* 6: 761-772.

Gruen, A. & Akca, D., 2005. Least squares 3D surface and curve matching. *ISPRS Journal of Photogrammetry and Remote Sensing 31 (3B)*, 151-174.

Gruen, A., Zhang, L. & Eisenbeiss, H., 2005. 3D Precision Processing of High-Resolution Satellite Imagery. *ASPRS 2005 Annual Conference,* Baltimore, Maryland, USA, March 7-11, on CD-ROM.

Kääb, A., Huggel, C., Barbero, S., Chiarle, M., Cordola, M., Epinfani, F., Haeberli, W., Mortara, G., Semino, P. Tamburini, A. & Viazzo, G., 2004. Glacier hazards at Belvedere glacier and the Monte Rosa east face, Italian Alps: Processes and mitigation. *Proceedings of the Interpraevent 2004* – Riva/Trient.

Leica Geospatial Imaging, LLC, *Leica Photogrammetry Suite Manager Guide*, 2006.

Vallet, J., 2007. GPS-IMU and LiDAR integration to aerial photogrammetry: Development and practical experiences with Helimap System®, *Voträge Dreiländertagung 27.*

Wissenschaftlich-Technische Jahrestagung der DGPF. 19-21 June 2007, Muttenz.

Vallet J. & Skaloud J., 2004. Development and Experiences with A Fully-Digital Handheld Mapping System Operated From A Helicopter, *The International Archives of the Photogrammetry, Remote Sensing and Spatial Information Sciences*, Istanbul, Vol. XXXV, Part B, Commission 5.

Wolff, D. & Gruen, A., 2007. DSM Generation from early ALOS/PRISM data using SAT-PP. *ISPRS Hannover Workshop "High-Resolution Earth Imaging for Geospatial Information"*, Hannover, Germany, 29 May-1 June.

Zhang, L., 2005. Automatic Digital Surface Model (DSM) Generation from Linear Array Images. Ph.D. Dissertation, Report No. 88, Institute of Geodesy and Photogrammetry, ETH Zurich, Switzerland.

Zhang, L. & Gruen, A., 2006. Multi-image Matching for DSM Generation from IKONOS Imagery. *ISPRS Journal of Photogrammetry and Remote Sensing,* Vol. 60, No.3, 195-211. Z/I Imaging Corporation, Image Station Digital Mensuration (04.04) Help, November 2004.